
Article:
Ruderman, M.S. orcid.org/0000-0003-2324-8466 and Petrukhin, N.S. (2021) Excitation of decayless kink oscillations by random motion. Monthly Notices of the Royal Astronomical Society, 501 (2). pp. 3017-3029. ISSN 0035-8711

https://doi.org/10.1093/mnras/staa3816

Monthly Notices of the ROYAL ASTRONOMICAL SOCIETY

MNRAS **501,** 3017–3029 (2021) doi:10.1093/mnras/staa3816
Advance Access publication 2020 December 12

Excitation of decayless kink oscillations by random motion

M. S. Ruderman[1,2]★ and N. S. Petrukhin[3]★

[1]*School of Mathematics and Statistics (SoMaS), The University of Sheffield, Hicks Building, Hounsfield Road, Sheffield S3 7RH, UK*
[2]*Space Research Institute (IKI) Russian Academy of Sciences, Moscow 117997, Russia*
[3]*National Research University Higher School of Economics, Moscow 101000, Russia*

Accepted 2020 December 7. Received 2020 December 5; in original form 2020 September 7

ABSTRACT

We study kink oscillations of a straight magnetic tube with a transitional region at its boundary. The tube is homogeneous in the axial direction. The plasma density monotonically decreases in the transitional region from its value inside the tube to that in the surrounding plasma. The plasma motion is described by the linear magnetohydrodynamic equations in the cold plasma approximation. We use the ideal equations inside the tube and in the surrounding plasma, but take viscosity into account in the transitional region. We also use the thin tube and thin transitional or boundary layer (TTTB) approximation. Kink oscillations are assumed to be driven by a driver at the tube footpoint. We derive the equation describing the displacement in the fundamental mode and overtones. We use this equation to study kink oscillations in both the case of harmonic and random driving. In the case of random driving, we assume that the driver is described by a stationary random function. The displacements in the fundamental mode and overtones are also described by stationary random functions. We derive the relation between the power spectra of the fundamental mode and all overtones and the power spectrum of the driver. We suggest a new method of obtaining information on the internal structure of coronal magnetic loops based on the shape of graphs of the power spectrum of the fundamental mode.

Key words: MHD – plasmas – waves – Sun: corona – Sun: oscillations.

1 INTRODUCTION

Transverse oscillations of coronal magnetic loops were first observed by the Transition Region And Coronal Explorer (TRACE) mission in 1998. These observations were reported by Aschwanden et al. (1999) and Nakariakov et al. (1999) and interpreted as kink oscillations of magnetic flux tubes. Now these oscillations are routinely observed by space missions (e.g. Erdélyi & Taroyan 2008; Duckenfield et al. 2018; Su et al. 2018; Abedini 2018; and references therein). The kink oscillations were also observed in prominence threads (e.g. Arregui, Oliver & Ballester 2018).

Transverse oscillations of coronal magnetic loops observed by TRACE had large amplitudes and were quickly damped. Later low-amplitude undamped or decayless transverse oscillations of coronal loops were observed (Tian et al. 2012; Wang et al. 2012; Nisticò, Nakariakov & Verwichte 2013; Nisticò, Anfinogentov & Nakariakov 2014; Anfinogentov, Nakariakov & Nisticò 2015). Recently, Duckenfield et al. (2018) reported the observation of multiple harmonics in decayless observations.

Since the decayless oscillations are ubiquitously present in the corona the question arises if they can provide the energy necessary to heat the corona. This problem was addressed by Hillier, Van Doorsselaere & Karampelas (2020). They assumed that there is a fully developed stationary turbulence in the transitional layer connecting the tube core and the surrounding plasma. This turbulence is caused by the Kelvin–Helmholtz (KH) instability. They obtained the relation between the amplitude of the loop kink oscillations and the amount of energy dissipated in the transitional layer. Using the observed amplitudes of the decayless kink oscillations they found that the amount of dissipated energy is insufficient to cover the radiative losses from coronal loops.

Two models of excitation of decayless coronal loop transverse oscillations were suggested. Nisticò et al. (2013, 2014) suggested that these oscillations are excited by random driving, most probably of the loop footpoints, by subphotospheric convective motion. Nakariakov et al. (2016) developed the model of decayless transverse oscillations as a nonlinear self-oscillatory process.

Afanasyev, Karampelas & Van Doorsselaere (2019) and Karampelas et al. (2019) studied the excitation of kink oscillations in a stratified coronal loop by a continuous monochromatic driving using the three-dimensional numerical modelling. They used a few driving frequencies. They found that for the same driving amplitude the excitation of kink waves is much more efficient when the deriving frequency is equal or close to the frequency either the fundamental mode or one of the frequencies of overtones, which is an expected result. They also found the manifestation of the KH instability that results in the development of turbulence in the transitional layer between the tube core region and the surrounding plasma. Thus, they confirmed the result previously found by other authors (e.g. Terradas et al. 2008; Terradas, Magyar & Van Doorsselaere 2018; Antolin, Yokoyama & Van Doorsselaere 2014; Antolin et al. 2016). However, it is doubtful that the decayless kink oscillations are excited by a harmonic driver. It looks like a more viable assumption that they are excited by the random driving.

The random driving was studied by De Groof, Tirry & Goossens (1998) and De Groof & Goossens (2000, 2002) mainly with the relation to the coronal loop heating. These authors modelled a

★ E-mail: M.S.Ruderman@sheffield.ac.uk (MSR); npetruhin@hse.ru (NSP)

coronal magnetic loop as a magnetic slab. Since the properties of kink oscillations of magnetic slabs and cylinders are quite different their analysis cannot be directly applied to the problem of excitation of decayless kink oscillations of coronal loops.

Recently, Afanasyev, Van Doorsselaere & Nakariakov (2020) studied the excitation of decayless kink oscillations of coronal loops by random motions using an inhomogeneous wave equation with damping and random driving. They managed to reproduce many observed properties of decayless kink oscillations like peaks in the Fourier spectrum of oscillations corresponding to the fundamental mode of the loop kink oscillation and its overtones. Our study is motivated by this article.

In this paper, we study the excitation of decayless oscillations by random motion modelling a coronal loop as a straight homogeneous magnetic tube with a transitional or boundary layer. The paper is organized as follows. In the next section, we formulate the problem. In Section 3.2, we solve the magnetohydrodynamic (MHD) equations in the tube transitional layer and calculate the variations of the radial plasma displacement and magnetic pressure perturbation across the transitional layer. In Section 4, we derive the governing equation for driven kink oscillations of the magnetic tube. In Section 5, we study the kink oscillations of the tube in the case of harmonic driving, while in Section 6 we study these oscillations in the case of stochastic driving. Section 7 contains the summary of the results and our conclusions.

2 PROBLEM FORMULATION AND GOVERNING EQUATIONS

We consider kink oscillations of a straight magnetic tube with a transitional layer at its boundary in the cold plasma approximation. The unperturbed magnetic field is straight. In cylindrical coordinates r, ϕ, z, it is given by $\mathbf{B} = B\mathbf{e}_z$, where $\mathbf{e}_z$ is the unit vector in the z-direction and B is a constant. The equilibrium plasma density is given by

$$\rho(r) = \begin{cases} \rho_i, & r \le R(1-\ell/2), \\ \rho_t(r), & R(1-\ell/2) \le r \le R(1+\ell/2), \\ \rho_e, & r \ge R(1+\ell/2), \end{cases} \tag{1}$$

where R is the tube radius, ρ_i and ρ_e are constants, $\rho_e < \rho_i$, $\rho_t(r)$ is a monotonically decreasing function, and $\rho(r)$ is continuous at $r = R(1 \pm \ell/2)$. The domain defined by $r \le R(1-\ell/2)$ is the core part of the magnetic tube, while $R(1-\ell/2) \le r \le R(1+\ell/2)$ is the transitional or boundary layer.

The tube length is L. We assume that the tube is thin, $R \ll L$. In addition, we assume that the transitional layer is also thin, $\ell \ll 1$. Hence, we use the thin tube and thin boundary layer (TTTB) approximation.

Ruderman, Shukhobodskiy & Erdélyi (2017) derived a very general equation describing kink oscillations of magnetic tubes in the TTTB and cold plasma approximations. This equation takes into account the tube expansion, the density variation along the tube, the presence of siphon plasma flow, and the time dependence of the plasma density. In the case when there is no equilibrium flow, the tube has constant cross-section radius, the density is independent of time, and the tube is homogeneous in the longitudinal direction this equation reduces to

$$\frac{\partial^2\eta}{\partial t^2} - C_k^2\frac{\partial^2\eta}{\partial z^2} = \frac{\mathcal{L}}{\rho_i+\rho_e}, \quad C_k^2 = \frac{2B^2}{\mu_0(\rho_i+\rho_e)}, \tag{2}$$

where

$$\mathcal{L} = \frac{\delta P}{R} + \frac{B^2}{\mu_0}\frac{\partial^2(\ell\eta+\delta\eta)}{\partial z^2} - \rho_e\frac{\partial^2(\ell\eta+\delta\eta)}{\partial t^2}. \tag{3}$$

When writing the expression for $\mathcal{L}$ we corrected a misprint in Ruderman et al. (2017) where the first term on the right-hand side of this expression is divided by R^2. In this equations μ_0 is the magnetic permeability of free space, η is the plasma displacement in the tube core orthogonal to the equilibrium magnetic field and in planes containing the tube axis, and P is the magnetic pressure perturbation; $\delta\eta$ and δP are the variations of the radial plasma displacement and magnetic pressure perturbation across the transitional layer defined by

$$\begin{aligned} \delta\eta &= \xi_r\big|_{r=R(1+\ell/2)} - \xi_r\big|_{r=R(1-\ell/2)}, \\ \delta P &= P\big|_{r=R(1+\ell/2)} - P\big|_{r=R(1-\ell/2)}, \end{aligned} \tag{4}$$

where ξ_r is the radial plasma displacement. We note that the radial plasma displacement in the tube core is independent of r and $\eta = \xi_r$ for $r \le R(1-\ell/2)$.

The tube ends are assumed to be frozen in the dense plasma that mimics the solar photosphere. For simplicity, we assume that one of the loop ends is immovable, while the other loop is driven and the driver is independent of r. Hence,

$$\eta = f(t) \quad \text{at} \quad z = 0, \quad \eta = 0 \quad \text{at} \quad z = L, \tag{5}$$

where, at present, $f(t)$ is arbitrary. Equation (2) with the right-hand side defined by equation (3) does not provide the full description of kink oscillations because it contains the quantities $\delta\eta$ and δP. To obtain this full description, it is necessary to express $\delta\eta$ and δP in terms of η.

3 SOLUTION IN TRANSITIONAL LAYER

The set of equations describing the plasma motion in the transitional layer in the cold plasma approximation are given by Shukhobodskiy & Ruderman (2018) (see equations 17–19). In the case of straight magnetic tube, this system reduces to

$$P = -\frac{B^2}{r\mu_0}\left(\frac{\partial(r\xi_r)}{\partial r} + \frac{\partial\xi_\phi}{\partial\phi}\right), \tag{6}$$

$$\frac{\partial^2\xi_r}{\partial t^2} = -\frac{1}{\rho}\frac{\partial P}{\partial r} + V_A^2\frac{\partial^2\xi_r}{\partial z^2} + \nu\frac{\partial}{\partial t}\left(\frac{\partial^2\xi_r}{\partial r^2} + \frac{1}{r^2}\frac{\partial^2\xi_r}{\partial\phi^2}\right), \tag{7}$$

$$\frac{\partial^2\xi_\phi}{\partial t^2} = -\frac{1}{r\rho}\frac{\partial P}{\partial\phi} + V_A^2\frac{\partial^2\xi_\phi}{\partial z^2} + \nu\frac{\partial}{\partial t}\left(\frac{\partial^2\xi_\phi}{\partial r^2} + \frac{1}{r^2}\frac{\partial^2\xi_\phi}{\partial\phi^2}\right), \tag{8}$$

where $V_A^2 = B^2/\mu_0\rho$ is the square of the Alfvén speed, ξ_ϕ is the azimuthal component of plasma displacement, and ν is the kinematic viscosity.

The characteristic length in the radial direction is R, while the characteristic length in the axial direction is L. This observation inspires us to introduce the scaled variable in the z-direction, $Z = \epsilon z$, where $\epsilon = R/L \ll 1$. The characteristic time calculated using the characteristic scale in the radial direction is R/V_{Ai}, where V_{Ai} is the Alfvén speed in the tube core. The typical period of kink oscillations is of the order of L/V_{Ai}. In accordance with this, we introduce the scaled time $T = \epsilon t$. It follows from equation (7) that P is of the order of $\epsilon^2\rho V_{Ai}^2(\xi_r/R)$. In accordance with this estimate, we introduce the scaled magnetic pressure perturbation $Q = \epsilon^{-2}P$. The terms proportional to ν in equations (7) and (8) describe the effect of viscosity. We assume that plasma is only weakly dissipative, which implies that the terms proportional to ν are only important where there are large gradients. We will see that these large gradients are

only present in the radial direction. This means that we can neglect terms with the derivatives with respect to ϕ in terms proportional to v. Now we assume that the driving is extended to the transitional layer, which implies that $\xi_r = f(t)$. Then we introduce

$$\tilde{\xi}_r = \xi_r + f(t)\frac{Z-R}{R}. \tag{9}$$

Now $\tilde{\xi}_r$ satisfies the boundary condition

$$\tilde{\xi}_r = 0 \quad \text{at} \quad Z = 0, R. \tag{10}$$

We also introduce

$$\tilde{\xi}_\phi = \xi_\phi + if(t)\frac{Z-R}{R}. \tag{11}$$

Since we study kink oscillations, we take all variables proportional to $e^{i\phi}$. In principle, it is possible to study a more general problem with all variables proportional to $e^{im\phi}$, where m is an arbitrary non-zero integer number, $|m| > 1$ corresponding to a fluting mode. However, no observations of fluting modes have been reported up to now. Since we study a linear problem and the equilibrium state is axisymmetric, there is no interaction between kink and fluting modes. Therefore, we restrict our analysis to kink modes and do not consider the fluting modes. Next, we rewrite equations (6)–(8) using the scaled variables and only keep terms of the leading order approximation with respect to ϵ. As a result, we obtain

$$\frac{\partial(r\tilde{\xi}_r)}{\partial r} + i\tilde{\xi}_\phi = 0, \tag{12}$$

$$\frac{\partial^2\tilde{\xi}_r}{\partial T^2} - V_A^2\frac{\partial^2\tilde{\xi}_r}{\partial Z^2} = \frac{Z-R}{R}\frac{\mathrm{d}^2 f}{\mathrm{d}t^2} - \frac{1}{\rho}\frac{\partial Q}{\partial r} + \bar{\nu}\frac{\partial^3\tilde{\xi}_r}{\partial T\partial r^2}, \tag{13}$$

$$\frac{\partial^2\tilde{\xi}_\phi}{\partial T^2} - V_A^2\frac{\partial^2\tilde{\xi}_\phi}{\partial Z^2} = i\frac{Z-R}{R}\frac{\mathrm{d}^2 f}{\mathrm{d}t^2} - \frac{iQ}{r\rho} + \bar{\nu}\frac{\partial^3\tilde{\xi}_\phi}{\partial T\partial r^2}, \tag{14}$$

where $\bar{\nu} = \epsilon^{-1}\nu$. It follows from equation (12) that $\tilde{\xi}_\phi$ satisfies the same boundary conditions as $\tilde{\xi}_r$. We also impose that Q satisfies the same boundary conditions.

Since $\tilde{\xi}_r$, $\tilde{\xi}_\phi$, and Q satisfy the zero boundary conditions, we can expand these variables in the Fourier series,

$$\tilde{\xi}_r = \sum_{n=1}^{\infty} u_n(r,T)\sin\frac{\pi n Z}{R}, \tilde{\xi}_\phi = \sum_{n=1}^{\infty} v_n(r,T)\sin\frac{\pi n Z}{R},$$
$$Q = \sum_{n=1}^{\infty} Q_n(r,T)\sin\frac{\pi n Z}{R}. \tag{15}$$

These expansions explicitly show that we consider standing waves. Substituting these expansions in equations (12)–(14) and using the identity

$$\frac{Z-R}{R} = -\frac{2}{\pi}\sum_{n=1}^{\infty}\frac{1}{n}\sin\frac{\pi n Z}{R}, \tag{16}$$

yields

$$\frac{\partial(ru_n)}{\partial r} + iv_n = 0, \tag{17}$$

$$\frac{\partial^2 u_n}{\partial T^2} + n^2\Omega_A^2 u_n - \bar{\nu}\frac{\partial^3 u_n}{\partial T\partial r^2} = -\frac{1}{\rho}\frac{\partial Q_n}{\partial r} - \frac{2}{\pi n}\frac{\mathrm{d}^2 f}{\mathrm{d}T^2}, \tag{18}$$

$$\frac{\partial^2 v_n}{\partial T^2} + n^2\Omega_A^2 v_n - \bar{\nu}\frac{\partial^3 v_n}{\partial T\partial r^2} = -\frac{iQ_n}{r\rho} - \frac{2i}{\pi n}\frac{\mathrm{d}^2 f}{\mathrm{d}T^2}, \tag{19}$$

where

$$\Omega_A = \frac{\pi V_A}{R}. \tag{20}$$

3.1 Solution to equation (19)

We consider the initial value problem for equation (19). For simplicity, we assume that

$$v_n = \frac{\partial v_n}{\partial T} = 0 \quad \text{at} \quad T = T_0. \tag{21}$$

We need to calculate $\delta\eta$ and δP in the leading order approximation with respect to $\ell \ll 1$. Hence, we can substitute R for r in equation (19). It follows from equation (18) that the relative variation of Q_n across the transitional layer is of the order of ℓ meaning that Q_n is almost constant in the transitional layer. In accordance with this we substitute Q_{ni} for Q_n in equation (19), where Q_{ni} is equal to Q_n at $r = R(1-\ell/2)$.

To solve equation (19) we use the method used by Ruderman (1999) to study the heating of coronal magnetic loops by phase-mixed torsional Alfvén waves. The ratio of the second term on the left-hand side of equation (19) to the third term is of the order of Reynolds number $\mathrm{Re} = RV_{Ai}/\bar{\nu}$; however, we will see later that this estimate is only valid for not very large time. The meaning of condition 'not very large time' will be specified later. We assume that $\mathrm{Re} \gg 1$. Then, for not very large time, the third term on the left-hand side of equation (19) can be neglected and it reduces to

$$\frac{\partial^2 v_n}{\partial T^2} + n^2\Omega_A^2 v_n = -ig_n(T), \tag{22}$$

where

$$g_n(T) = \frac{Q_{ni}}{\rho R} + \frac{2}{\pi n}\frac{\mathrm{d}^2 f}{\mathrm{d}T^2}. \tag{23}$$

The solution to this equation satisfying the initial conditions equation (21) is

$$v_n = \frac{i}{n\Omega_A}\int_{T_0}^{T} g_n(T')\sin[n\Omega_A(T'-T)]\,\mathrm{d}T'. \tag{24}$$

Differentiating this expression with respect to r yields

$$\frac{\partial v_n}{\partial r} = \frac{i}{\Omega_A}\frac{\mathrm{d}\Omega_A}{\mathrm{d}r}\int_{T_0}^{T}(T'-T)g_n(T') \times\cos[n\Omega_A(T'-T)]\,\mathrm{d}T' + \ldots, \tag{25}$$

where '...' indicates terms not growing with time. We can see that the derivative of v_n with respect to r increases unboundedly in time. This implies that after sufficiently large time the third term on left-hand side of equation (19) will be of the same order as the two other terms. Hence, the approximate solution to equation (19) given by equation (24) is not uniformly valid.

To obtain the uniformly valid approximate solution to equation (19), we use the Wentzel-Kramers-Brillouin (WKB) method (e.g. Bender & Orszag 1999). The first step is to find the solution to the homogeneous counterpart of equation (19). To do this we introduce the 'slow' time $\tau = \alpha(T - T_0)$, where $\alpha \ll 1$. Then we look for the solution to the homogeneous counterpart of equation (19) in the form $v_n = U(r,\tau)\exp[i\alpha^{-1}\Theta(r,\tau)]$. Substituting this expression in the homogeneous counterpart of equation (19), we obtain

$$U\left(\frac{\partial\Theta}{\partial\tau}\right)^2 - n^2\Omega_A^2 U - 2i\alpha\frac{\partial\Theta}{\partial\tau}\frac{\partial U}{\partial\tau} - i\alpha U\frac{\partial^2\Theta}{\partial\tau^2} - i\alpha^{-2}\bar{\nu}U\frac{\partial\Theta}{\partial\tau}\left(\frac{\partial\Theta}{\partial r}\right)^2 = \mathcal{O}(\alpha^2) + \mathcal{O}(\alpha^{-1}\bar{\nu}). \tag{26}$$

Now, we assume that the third and fifth terms on the lest-hand side of this equation are of the same order. To satisfy this condition, we take $\alpha = \mathrm{Re}^{-1/3}$. In the first-order approximation (the approximation

of geometrical optics), we collect terms of the order of unity in equation (26) to obtain

$$\frac{\partial \Theta}{\partial \tau} = \pm n\Omega_A. \tag{27}$$

For simplicity, we take $\Theta = 0$ at $\tau = 0$. Then it follows from equation (27) that

$$\Theta = \pm n\Omega_A \tau. \tag{28}$$

In the second-order approximation (the approximation of physical optics), we collect terms of the order of α in equation (26). Then, using equation (28) we obtain

$$\frac{\partial U}{\partial \tau} = -3\Lambda n^2 \tau^2 U, \quad \Lambda = \frac{RV_{Ai}}{6\mathrm{Re}} \left(\frac{\mathrm{d}\Omega_A}{\mathrm{d}r}\right)^2. \tag{29}$$

It follows from this equation that

$$U = U_0(r) \exp(-\Lambda n^2 \tau^3), \tag{30}$$

where $U_0(r)$ is an arbitrary function. The general solution to the homogeneous counterpart of equation (19) is the linear combination of two linearly independent solutions, one corresponding to the plus sign in equation (28) and the other to the minus sign. Returning to the original variable, we write this solution as

$$v_n = \exp[-\Lambda n^2 (T - T_0)^3/\mathrm{Re}]\{A_c(r)\cos[n\Omega_A(T - T_0)] + A_s(r)\sin[n\Omega_A(T - T_0)]\}, \tag{31}$$

where $A_c(r)$ and $A_s(r)$ are arbitrary functions.

Now, we obtain the solution to equation (19) satisfying the initial conditions equation (21). To do this we construct Green's function $\overline{G}_n(T, \theta)$. Considered as a function of T it must satisfy the homogeneous counterpart of equation (19), be continuous, and also satisfy the conditions

$$\overline{G}_n(T, \theta) = 0 \quad \text{for} \quad T < \theta, \quad \lim_{T \to \tau + 0} \frac{\partial \overline{G}_n}{\partial T} = 1. \tag{32}$$

It is easy to verify that the function $\overline{G}_n(T, \theta) = G_n(T - \theta)$, where

$$G_n(T) = H(T) \exp(-\Lambda n^2 T^3/\mathrm{Re}) \frac{\sin(n\Omega_A T)}{n\Omega_A}, \tag{33}$$

satisfies all these conditions. In equation (33) $H(T)$ is the Heaviside step function, $H(T) = 0$ for $T < 0$, $H(T) = 1$ for $T > 0$. In particular, since $G_n(T) = 0$ for $T < 0$, it follows that $\overline{G}_n(T, \theta) = G_n(T - \theta) = 0$ for $T < \theta$. Then the convolution of $G_n(T)$ and $-ig_n(T)$ gives a particular solution to equation (19). It is straightforward to show that this solution satisfies the initial conditions equation (21). Now, taking $T_0 \to -\infty$, we obtain

$$v_n = -i \int_{-\infty}^{T} G_n(T - \theta) g_n(\theta)\, \mathrm{d}\theta. \tag{34}$$

3.2 Calculation of $\delta\eta$ and δP

Using equations (4), (9), (12), (15), and (34), and the approximation $r \approx R$ yields

$$\delta\eta_n = -\frac{1}{R} \int_{R(1-\ell/2)}^{R(1+\ell/2)} \mathrm{d}r \int_{-\infty}^{T} G_n(T - \theta) g_n(\theta)\, \mathrm{d}\theta, \tag{35}$$

where $\delta\eta_n$ is the coefficient of expansion of $\delta\eta$ in the Fourier series similar to those given by equation (15). We note that, since $f(t)$ is independent of r, $\delta\eta = 0$ at $z = 0, L$ and, consequently, $\delta\eta = 0$ can be expanded in the Fourier series with respect to z.

Next, we calculate δP in the leading order approximation with respect to ℓ and Re^{-1}. We use the relation $P = \epsilon^2 Q$ and the expansion of Q in the Fourier series given by equation (15). Even after the phase mixing creates small scales in the radial direction in the transitional layer the ratio of the third term on the left-hand side of equation (18) to the second term is of the order of $\mathrm{Re}^{-1/3}$. Hence, we can neglect the third term when calculating the variation of Q_n across the transitional layer. Since the ratio of variation of u_n across the transitional layer to its value at $r = R(1 - \ell/2)$ is of the order of ℓ we can substitute the value of u_n at $r = R(1 - \ell/2)$ in equation (18) when calculating the variation of Q_n. Expanding η in the Fourier series similar to those given by equation (15), using equations (9) and (16), and taking into account that $\xi_r = \eta$ in the core region we obtain

$$u_n\big|_{r=R(1-\ell/2)} = \eta_n, \tag{36}$$

where η_n are the Fourier coefficients of expansion of $\eta + f(t)(Z - R)/R$. Now, equation (18) reduces to the approximate form

$$\frac{1}{\rho}\frac{\partial Q_n}{\partial r} = -\frac{2}{\pi n}\frac{\mathrm{d}^2 f}{\mathrm{d}T^2} - \frac{\mathrm{d}^2\eta_n}{\mathrm{d}T^2} - n^2\Omega_A^2\eta_n, \tag{37}$$

where Ω_{Ai} is the value of Ω_A at $r = R(1 - \ell/2)$. Then the coefficients of the Fourier expansion of δP are given by

$$\delta P_n = -\epsilon^2 \left[\left(\frac{2}{\pi n}\frac{\mathrm{d}^2 f}{\mathrm{d}T^2} + \frac{\mathrm{d}^2\eta_n}{\mathrm{d}T^2} \right) \int_{R(1-\ell/2)}^{R(1+\ell/2)} \rho(r)\, \mathrm{d}r + \ell R \rho \Omega_A^2 n^2 \eta_n \right]. \tag{38}$$

When deriving this equation, we used the approximation $r \approx R$. We also use this approximation below when calculating integrals with respect to r over the transitional layer.

We need the expressions of $\delta\eta$ and δP in terms of η. However, the expression for $\delta\eta_n$ involves Q_{ni}, which is the value of Q_n at $r = R(1 - \ell/2)$. We note that equations (17)–(19) are valid not only in the transitional layer but also in the core region. Since there are no large gradients in the core region, we can safely neglect the terms proportional to $\bar{v}$. Since ξ_r is independent of r in the core region, we obtain from equation (17) that

$$v_n = i\eta_n. \tag{39}$$

Substituting this expression in equation (19) and taking $r \approx R$, we obtain

$$Q_{ni} = -\rho_i R \left(\frac{\mathrm{d}^2\eta_n}{\mathrm{d}T^2} + n^2\Omega_{Ai}^2\eta_n + \frac{2}{\pi n}\frac{\mathrm{d}^2 f}{\mathrm{d}T^2} \right). \tag{40}$$

Substituting this expression in the expression for g_n given by equation (23) yields

$$g_n(T) = \frac{2(\rho - \rho_i)}{\pi n \rho}\frac{\mathrm{d}^2 f}{\mathrm{d}T^2} - \frac{\rho_i}{\rho}\left(\frac{\mathrm{d}^2\eta_n}{\mathrm{d}T^2} + n^2\Omega_{Ai}^2\eta_n \right). \tag{41}$$

Equations (33), (35), (38), and (41) determine the coefficients of Fourier expansions of $\delta\eta$ and δP.

4 DERIVATION OF GOVERNING EQUATION FOR η

Since $\mathcal{L}$ is of the order of ℓ it follows from equation (2) that

$$\frac{\mathrm{d}^2\eta}{\mathrm{d}t^2} = C_k^2 \frac{\mathrm{d}^2\eta}{\mathrm{d}z^2} + \mathcal{O}(\ell). \tag{42}$$

It follows from this equation that

$$\frac{\mathrm{d}^2\eta_n}{\mathrm{d}t^2} + \frac{2}{\pi n}\frac{\mathrm{d}^2 f}{\mathrm{d}t^2} = -\frac{\pi^2 n^2 C_k^2 \eta_n}{L^2}. \tag{43}$$

Using equation (42), we reduce equation (3) to the approximate form

$$\mathcal{L} = \frac{\delta P}{R} + \frac{\ell}{2} C_k^2 (\rho_i - \rho_e) \frac{\partial^2 \eta}{\partial z^2} + \frac{B^2}{\mu_0} \frac{\partial^2 \delta \eta}{\partial z^2} - \rho_e \frac{\partial^2 \delta \eta}{\partial t^2}. \tag{44}$$

Now, we obtain with the aid of equations (7), (38), and (43) that the Fourier coefficients of the expansion of $\mathcal{L}$ are given by

$$\mathcal{L}_n = \varpi_k^2 n^2 \eta_n \left(\frac{1}{R} \int_{R(1-\ell/2)}^{R(1+\ell/2)} \rho(r)\, \mathrm{d}r - \ell \rho_i \right) - \rho \omega_A^2 n^2 \delta \eta_n - \rho_e \frac{\mathrm{d}^2 \delta \eta_n}{\mathrm{d}t^2}, \tag{45}$$

where

$$\varpi_k = \frac{\pi C_k}{L}, \quad \omega_A = \epsilon \Omega_A = \frac{\pi V_A}{L}. \tag{46}$$

Substituting equation (45) in equation (2), we obtain

$$\frac{\mathrm{d}^2 \eta_n}{\mathrm{d}t^2} + n^2 \varpi_k^2 \eta_n \left[1 + \frac{1}{\rho_i + \rho_e} \left(\ell \rho_i - \frac{1}{R} \int_{R(1-\ell/2)}^{R(1+\ell/2)} \rho(r)\, \mathrm{d}r \right) \right] = -\frac{\rho_e}{\rho_i + \rho_e} \left(\omega_{Ae}^2 n^2 \delta \eta_n + \frac{\mathrm{d}^2 \delta \eta_n}{\mathrm{d}t^2} \right) - \frac{2}{\pi n} \frac{\mathrm{d}^2 f}{\mathrm{d}t^2}. \tag{47}$$

The second term in the square brackets only provides a slight correction of the order of ℓ to the frequency of the fundamental mode and overtones. This correction is related to the presence of the transitional layer. Usually, this correction is neglected when studying the damping of kink oscillations due to resonant absorption. We will do the same and also neglect this correction below. The expression for the first term on the right-hand side of equation (47) is obtained in Appendix A (see equation A22). Neglecting the second term and using equation (A22), we transform equation (47) to

$$\frac{\mathrm{d}^2 \eta_n}{\mathrm{d}t^2} + n^2 \varpi_k^2 \eta_n + \frac{\rho_e \rho_i n^6}{R(\rho_i + \rho_e)} (\varpi_k^2 - \omega_{Ae}^2)(\varpi_k^2 - \omega_{Ai}^2) \times \int_{R(1-\ell/2)}^{R(1+\ell/2)} \frac{\mathrm{d}r}{\rho} \int_{-\infty}^{t} \widetilde{G}_n(t-\theta) \eta_n(\theta)\, \mathrm{d}\theta = \frac{2 n \rho_e}{\pi R(\rho_i + \rho_e)} \int_{R(1-\ell/2)}^{R(1+\ell/2)} (\omega_{Ae}^2 - \omega_A^2)\, \mathrm{d}r \times \int_{-\infty}^{t} \widetilde{G}_n(t-\theta) \frac{\mathrm{d}^2 f}{\mathrm{d}\theta^2}\, \mathrm{d}\theta - \frac{2[\rho_i + (1-\ell)\rho_e]}{\pi n (\rho_i + \rho_e)} \frac{\mathrm{d}^2 f}{\mathrm{d}t^2}. \tag{48}$$

Using the identity

$$(\varpi_k^2 - \omega_{Ae}^2)(\varpi_k^2 - \omega_{Ai}^2) = -\frac{\varpi_k^2 (\rho_i - \rho_e)^2}{4 \rho_e \rho_i}, \tag{49}$$

and the expression for $\widetilde{G}_n(t-\theta)$ defined by equation (A4), we obtain that the last term on the left-hand side of equation (47) is equal to

$$\hat{L}[\eta_n] = -\frac{n^5 \varpi_k^2 (\rho_i - \rho_e)^2}{2R(\rho_i + \rho_e)^2} \int_{R(1-\ell/2)}^{R(1+\ell/2)} \omega_A\, \mathrm{d}r \times \int_{-\infty}^{t} \exp\left(-n^2 (t-\theta)^3 / t_\mathrm{d}^3\right) \sin[n \omega_A (t-\theta)] \eta_n(\theta)\, \mathrm{d}\theta, \tag{50}$$

where

$$t_\mathrm{d} = \left[\frac{\nu}{6} \left(\frac{\mathrm{d}\omega_A}{\mathrm{d}r} \right)^2 \right]^{-1/3}. \tag{51}$$

The ratio of the first term on the right-hand side of this equation to the second term is of the order of ℓ meaning that the first term can be neglected. We also can neglect ℓ in comparison with unity in the second term. Then finally we reduce equation (47) to

$$\frac{\mathrm{d}^2 \eta_n}{\mathrm{d}t^2} + n^2 \varpi_k^2 \eta_n + \hat{L}[\eta_n] = -\frac{2}{\pi n} \frac{\mathrm{d}^2 f}{\mathrm{d}t^2}. \tag{52}$$

5 HARMONIC DRIVING

In this section, we consider the excitation of kink oscillations of a magnetic tube by harmonic driving of its footpoint. This problem was extensively studied for a few decades (see e.g. Goossens, Erdélyi & Ruderman 2011 and references therein). Hence, we will present only a very brief analysis.

When we took the plasma displacement and the magnetic pressure perturbation proportional to $e^{i\phi}$, we implicitly assumed that these quantities are complex variables. Hence, only their real parts have the physical sense. This implies that we can also take $f(t)$ to be complex. In accordance with this, we take

$$f(t) = a \mathrm{e}^{i \omega_d t}, \tag{53}$$

where a and ω_d are real constants. Now, we look for the solution to equation (50) in the form $\eta_n = A_n \mathrm{e}^{i \omega_d t}$. With the aid of the variable substitution $\theta = t - t_d \tilde{\theta} (3n^2)^{-1/3}$, we obtain

$$\int_{-\infty}^{t} \exp\left(-n^2 (t-\theta)^3 / t_\mathrm{d}^3\right) \sin[n \omega_A (t-\theta)] \mathrm{e}^{i \omega_\mathrm{d} \theta}\, \mathrm{d}\theta = i \psi_n(\omega_d) \mathrm{e}^{i \omega_\mathrm{d} t}, \tag{54}$$

where

$$\psi_n(\omega) = \frac{t_d}{2(3n^2)^{1/3}} \left[F\left(t_d (3n^2)^{-1/3} (-\omega - n\omega_A)\right) - F\left(t_d (3n^2)^{-1/3} (-\omega + n\omega_A)\right) \right], \tag{55}$$

$$F(x) = \int_0^\infty \exp(i x \theta - \theta^3/3)\, \mathrm{d}\theta. \tag{56}$$

This function was first introduced by Goossens, Ruderman & Hollweg (1995) (see also Goossens et al. 2011). When deriving equation (54) we dropped the tilde. Substituting $\eta_n = A_n e^{i \omega_d t}$ in equation (50) yields

$$A_n \left[-\frac{i n^5 \varpi_k^2 (\rho_i - \rho_\mathrm{e})^2}{2R(\rho_i + \rho_\mathrm{e})^2} \int_{R(1-\ell/2)}^{R(1+\ell/2)} \omega_A \psi_n(\omega_\mathrm{d})\, \mathrm{d}r + \left(n^2 \varpi_k^2 - \omega_\mathrm{d}^2\right) \right] = \frac{2 a \omega_\mathrm{d}^2}{\pi n}. \tag{57}$$

Below we only consider moderate values of n implying that n can be considered as a quantity of the order of unity. First, we assume that there is no resonance between the driver and the nth harmonic. Moreover, we assume that $|\omega_d - n \varpi_k| \sim \varpi_k$. It is easy to show that the ratio of the first term to the second term in equation (57) is of the order of ℓ. Then we obtain

$$A_n = \frac{2 a \omega_d^2}{\pi n \left(n^2 \varpi_k^2 - \omega_d^2\right)} + \mathcal{O}(\ell). \tag{58}$$

Hence, in this case the amplitude of the nth harmonic is of the order of the driver amplitude.

It is instructive to compare the results of our analytical study with those obtained in the numerical modelling by Afanasyev et al. (2019). It is difficult to make the quantitative comparison for many reasons, not least because in the numerical modelling by Afanasyev et al. (2019) the loop was only driven for a few periods of the fundamental mode. It seems that after this time the system is in the state of quasi-stationary oscillation. To reach the state of stationary oscillation, one needs to drive the loop for longer time. Still the amplitude dependence on the driving frequency is qualitatively similar to that given by equation (58). The amplitude takes maximum when the driving frequency is equal to the fundamental frequency of kink oscillations, which is in the agreement with the result obtained below. The oscillation amplitude decays when $\omega_d > \varpi_k$ and increases,

although in fig. 2 in Afanasyev et al. (2019) this decay is non-monotonic.

Now, we consider the case where $|\omega_d - n\varpi_k| \sim \ell\varpi_k$. In this case, the first and second terms in the square brackets on the left-hand side of equation (57) are of the same order and we can expect that A_n is of the order of a/ℓ. We only consider the case of the exact resonance where $\omega_d = n\varpi_k$. It is shown in Appendix B that in this case

$$A_n = \frac{4aR(\rho_i+\rho_e)^2}{\pi n^5(\rho_i-\rho_e)^2}\left(\mathcal{P}\int_{R(1-\ell/2)}^{R(1+\ell/2)}\frac{\omega_\mathrm{A}^2\,\mathrm{d}r}{\varpi_k^2-\omega_\mathrm{A}^2}+\frac{i\pi\varpi_k}{4\Delta}\right)^{-1}, \tag{59}$$

where

$$\Delta = -\left.\frac{\mathrm{d}\omega_\mathrm{A}}{\mathrm{d}r}\right|_{r=r_\mathrm{A}}, \quad \omega_\mathrm{A}(r_\mathrm{A}) = \varpi_k, \tag{60}$$

r_A is the point of Alfvén resonance and $\mathcal{P}$ indicates that the integral is calculated in the sense of Cauchy principal part. Since the first term in the brackets in equation (59) is over the interval with the length ℓR, it follows that this term is of the order of ℓR. The characteristic scale of variation of ω_A in the transitional layer is ℓR. Since ω_A is of the order of ϖ_k, we conclude that Δ is of the order of $\varpi_k(\ell R)^{-1}$. Then it follows that the second term in the brackets in equation (59) is also of the order of ℓR. Using these estimates we obtain that A_n is of the order of a/ℓ as it was expected. The driver amplitude a is multiplied by a complex quantity. This implies that there is the phase shift of the kink oscillation in comparison with the driver phase. This phase shift is related to the presence of the Alfvén resonance.

We note that in this section we only considered the steady state of driven oscillation and did not study the transition to this state. When the driving begins the oscillation amplitude in the dissipative layer starts to grow. This growth continues until the amount of energy dissipated due to viscosity per one period of oscillation matches the amount of input energy. In this state, the oscillation amplitude is of the order of $\mathrm{Re}^{1/3}$ times the driver amplitude (e.g. Goossens et al. 1995, 2011).

6 STOCHASTIC DRIVING

6.1 General analysis

Now, we proceed to the main aim of this paper which is the stochastic driving of kink oscillations. We assume that $f(t)$ is a stationary random function. We introduce the Fourier transform

$$\hat{h}(\omega) = \mathcal{F}(h) \equiv \int_{-\infty}^{\infty} h(t)\mathrm{e}^{-i\omega t}\mathrm{d}t,$$
$$h(t) = \frac{1}{2\pi}\int_{-\infty}^{\infty}\hat{h}(\omega)\mathrm{e}^{i\omega t}\mathrm{d}\omega. \tag{61}$$

Stationary random functions do not possess the Fourier transform. Hence, following Champeney (1973) we introduce the truncated function

$$f_T(t) = \begin{cases} f(t), & T_1 < t < T+T_1, \\ 0, & \text{otherwise.}\end{cases} \tag{62}$$

Now we solve equation (50) with $f_T(t)$ substituted for $f(t)$. It is shown in Appendix C that

$$\mathcal{F}\left(\hat{L}[\eta_n]\right) = i\hat{\eta}_n(\omega)K(\omega), \tag{63}$$

where

$$K(\omega) = -\frac{n^5\varpi_k^2(\rho_i-\rho_e)^2}{2R(\rho_i+\rho_e)^2}\int_{R(1-\ell/2)}^{R(1+\ell/2)}\omega_A\psi_n(\omega)\,\mathrm{d}r \tag{64}$$

and $\psi_n(\omega)$ is defined by equation (55). We denote the corresponding solution to equation (50) as η_{Tn}. It is shown in Appendix C that equation (64) reduces to

$$K(\omega) = \frac{n^6\varpi_k^2(\rho_i-\rho_e)^2}{2R(\rho_i+\rho_e)^2}\left(\frac{\pi\omega}{4n^2\Delta_n} - \mathcal{P}\int_{R(1-\ell/2)}^{R(1+\ell/2)}\frac{i\omega_A^2\,\mathrm{d}r}{\omega^2-n^2\omega_A^2}\right) \tag{65}$$

for $\omega \in [n\omega_{Ai}, n\omega_{Ae}]$, and

$$K(\omega) = -\frac{n^6\varpi_k^2(\rho_i-\rho_e)^2}{2R(\rho_i+\rho_e)^2}\mathcal{P}\int_{R(1-\ell/2)}^{R(1+\ell/2)}\frac{i\omega_A^2\,\mathrm{d}r}{\omega^2-n^2\omega_A^2} \tag{66}$$

for $\omega \notin [n\omega_{Ai}, n\omega_{Ae}]$, where

$$\Delta_n = -n\left.\frac{\mathrm{d}\omega_A}{\mathrm{d}r}\right|_{r=r_n(\omega)}, \quad n\omega_A(r_n) = \omega. \tag{67}$$

We note that equations (65) and (66) are only valid when ω is not very close to $n\omega_{Ai}$ and $n\omega_{Ae}$, that is when $|\omega - n\omega_{Ai}| \gg \varpi_k(\ell^2\mathrm{Re})^{-1/3}$ and $|\omega - n\omega_{Ae}| \gg \varpi_k(\ell^2\mathrm{Re})^{-1/3}$.

Applying the Fourier transform to equation (50) with $f_T(t)$ substituted for $f(t)$ and using equation (63), we obtain

$$\hat{\eta}_{Tn}\left[n^2\varpi_k^2 - \omega^2 + iK(\omega)\right] = \frac{2\omega^2}{\pi n}\hat{f}_T. \tag{68}$$

Now, we define the power spectrum $P_f(\omega)$ as (Champeney 1973)

$$P_f(\omega) = \lim_{T\to\infty}\frac{1}{2T}|\hat{f}_T(\omega)|^2. \tag{69}$$

When $f(t)$ is a stationary random process this limit is independent of T_1. The amplitude of the nth harmonic, η_n, is also a stationary random process. Its power spectrum is defined by

$$P_{\eta_n}(\omega) = \lim_{T\to\infty}\frac{1}{2T}|\hat{\eta}_{Tn}(\omega)|^2 = |\Upsilon_n(\omega)|^2 P_f(\omega), \tag{70}$$

where

$$\Upsilon_n(\omega) = \frac{2\omega^2}{\pi n[n^2\varpi_k^2 - \omega^2 + iK(\omega)]}. \tag{71}$$

6.2 Linear density profile

We now introduce the characteristic scale of variation of $P_f(\omega)$, ω_ch, and assume that $\omega_\mathrm{ch} \gg \ell\varpi_k$. This condition is equivalent to the inequality

$$\left|\frac{\mathrm{d}P_f}{\mathrm{d}\omega}\right| \sim \frac{|P_f|}{\omega_\mathrm{ch}} \ll \frac{|P_f|}{\ell\varpi_k}. \tag{72}$$

In particular, this condition is satisfied for white noise because in this case $\mathrm{d}P_f/\mathrm{d}\omega = 0$. It follows from the condition imposed on $P_f(\omega)$ that we can take $P_f(\omega) \approx P_f(n\varpi_k)$ in the interval centred at $n\varpi_k$ and with the length of a few $\ell\varpi_k$. In accordance with this, we introduce

$$\Pi(\omega) = \frac{P_{\eta_n}(\omega)}{P_f(n\varpi_n)} = |\Upsilon_n(\omega)|^2. \tag{73}$$

Then we assume that the plasma density variation in the transitional layer is linear,

$$\rho(r) = \frac{\rho_i}{2\ell\zeta R}[\ell R(\zeta+1) - 2(r-R)(\zeta-1)], \tag{74}$$

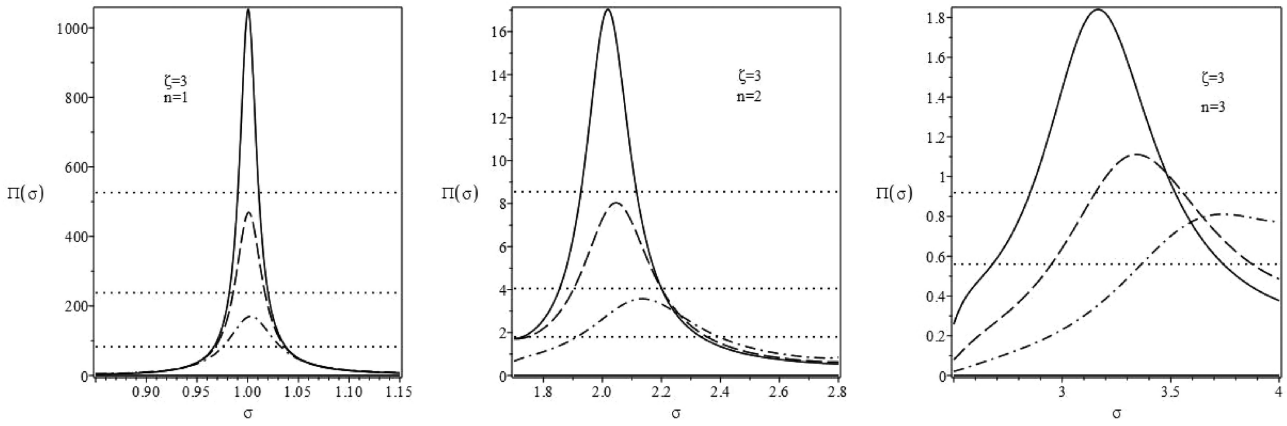

Figure 1. Dependence of Π on σ for $\zeta = 3$. The left, middle, and right-hand panels correspond to $n = 1$, 2, and 3, respectively. The solid, dashed, and dash–dotted curves correspond to $\ell = 0.1$, 0.15, and 0.25. The dotted horizontal lines show the levels corresponding to the half maximum of $\Pi(\sigma)$. We did not put the dotted line for the dash–dotted curve on the right-hand panel because the dash–dotted curve does not go below half of the maximum on the right-hand side on the figure.

where $\zeta = \rho_i/\rho_e$. A simple calculation yields

$$\mathcal{P}\int_{R(1-\ell/2)}^{R(1+\ell/2)} \frac{\omega_A^2\,\mathrm{d}r}{\omega^2 - n^2\omega_A^2} = \frac{\ell R(\zeta+1)}{2\sigma^2(\zeta-1)} \ln\left|\frac{2\zeta\sigma^2 - n^2(\zeta+1)}{2\sigma^2 - n^2(\zeta+1)}\right|, \tag{75}$$

where $\sigma = \omega/\varpi_k$. Substituting this expression in equations (65) and (66), we obtain

$$\widetilde{K}(\sigma) = -\frac{\ell n^6(\zeta-1)}{4\sigma^2(\zeta+1)}\left(\frac{\pi}{2} + i\ln\left|\frac{2\zeta\sigma^2 - n^2(\zeta+1)}{2\sigma^2 - n^2(\zeta+1)}\right|\right) \tag{76}$$

for

$$\sigma \in \left[n\left(\frac{\zeta+1}{2\zeta}\right)^{1/2}, n\left(\frac{\zeta+1}{2}\right)^{1/2}\right], \tag{77}$$

$$\widetilde{K}(\sigma) = -\frac{i\ell n^6(\zeta-1)}{4\sigma^2(\zeta+1)} \ln\left|\frac{2\zeta\sigma^2 - n^2(\zeta+1)}{2\sigma^2 - n^2(\zeta+1)}\right| \tag{78}$$

for

$$\sigma \notin \left[n\left(\frac{\zeta+1}{2\zeta}\right)^{1/2}, n\left(\frac{\zeta+1}{2}\right)^{1/2}\right], \tag{79}$$

where $\widetilde{K}(\sigma) = \varpi_k^{-2}K(\sigma)$. The condition given by equation (77) means that σ is in the Alfvén continuum of the nth harmonic of kink oscillations. It is obvious that $|\Upsilon_n(\sigma)|$ takes a minimum when σ is sufficiently close to n, which implies that σ satisfies equation (77). In this case, we have

$$|\Upsilon_n(\sigma)|^2 = \frac{4\sigma^4}{\pi^2 n^2}\left[\frac{\pi^2\ell^2 n^{12}(\zeta-1)^2}{64\sigma^4(\zeta+1)^2} + \left(n^2 - \sigma^2 + \frac{\ell n^6(\zeta-1)}{4\sigma^2(\zeta+1)}\ln\left|\frac{2\zeta\sigma^2 - n^2(\zeta+1)}{2\sigma^2 - n^2(\zeta+1)}\right|\right)^2\right]^{-1}. \tag{80}$$

Since the first term in the square brackets is of the order of ℓ^2 and the second term is zero when $\sigma = n$, it follows that $|\Upsilon_n(\sigma)|^2$ takes a maximum when $\sigma = n + \mathcal{O}(\ell)$ and this maximum is

$$\max[\Pi(\sigma)] = \frac{256(\zeta+1)^2}{\ell^2\pi^4 n^6(\zeta-1)^2} + \mathcal{O}\left(\ell^{-1}\right). \tag{81}$$

The dependence of Π on σ given by equations (73) and (80) is shown in Figs. 1 and 2 for $n = 1$, 2, 3. Fig. 1 corresponds to $\zeta = 3$, and Fig. 2 to $\zeta = 10$, where $\zeta = \rho_i/\rho_e$.

We now calculate the width of the graph of $\Pi(\sigma)$ at the half of its height. It is defined by

$$\delta\sigma = \sigma_+ - \sigma_-, \quad \Pi(\sigma_\pm) = \frac{1}{2}\max[\Pi(\sigma)]. \tag{82}$$

We put $\sigma_\pm = n + \ell\tilde{\sigma}_\pm$ and assume that $\tilde{\sigma}_\pm$ is of the order of unity. Then, using equations (73), (80), and (81), we obtain from equation (82) in the leading order approximation

$$\tilde{\sigma}_\pm \pm \frac{\pi n^3(\zeta-1)}{16(\zeta+1)}. \tag{83}$$

As a result, we obtain

$$\delta\sigma = \ell(\tilde{\sigma}_+ - \tilde{\sigma}_-) = \frac{\pi\ell n^3(\zeta-1)}{8(\zeta+1)}. \tag{84}$$

We observe in Figs. 1 and 2 that $\Pi(\sigma)$ takes maximum at $\sigma = 1$ and equation (81) is quite accurate for $n = 1$. However, this is not the case for $n = 2$ and $n = 3$. The point where $\Pi(\sigma)$ takes local maximum is shifted to the right from $\sigma = n$ when $n = 2$ and $n = 3$. This shift is more pronounced for $n = 3$ and it increases with the increase in ℓ, which is not surprising because the ratio of the second term on the right-hand side of equation (81) increases with the increase in ℓ. Finally, the shift of the point where $\Pi(\sigma)$ takes a local maximum and the deviation of this maximum from the value given by equation (81) is also more pronounced for smaller values of ζ.

When a kink oscillation of a coronal loop is caused by an impulsive excitation like a nearby solar flare, the ratio of frequency of the first overtone to that of the fundamental harmonic must be 2 if the loop is homogeneous in the longitudinal direction. Verwichte et al. (2004) reported the first observation of both fundamental mode and first overtone of coronal loop kink oscillations. They found that the frequency ratio was less than 2. Andries, Arregui & Goossens (2005) suggested that this deviation of the ratio from 2 was caused by the variation of the density along the loop (see also Arregui et al. 2007). They then developed a method for estimating the atmospheric scale height using the ratio of frequencies of the first overtone and fundamental harmonic. Later this method was extended to take the loop expansion into account (Ruderman, Verth & Erdélyi 2008; Verth & Erdélyi 2008; Verth, Erdélyi & Jess 2008; see also the review by Andries et al. 2009). Recently, Duckenfield et al. (2018) reported the detection of the first overtone in decayless kink oscillations of coronal loops. This implies that decayless kink oscillations can also

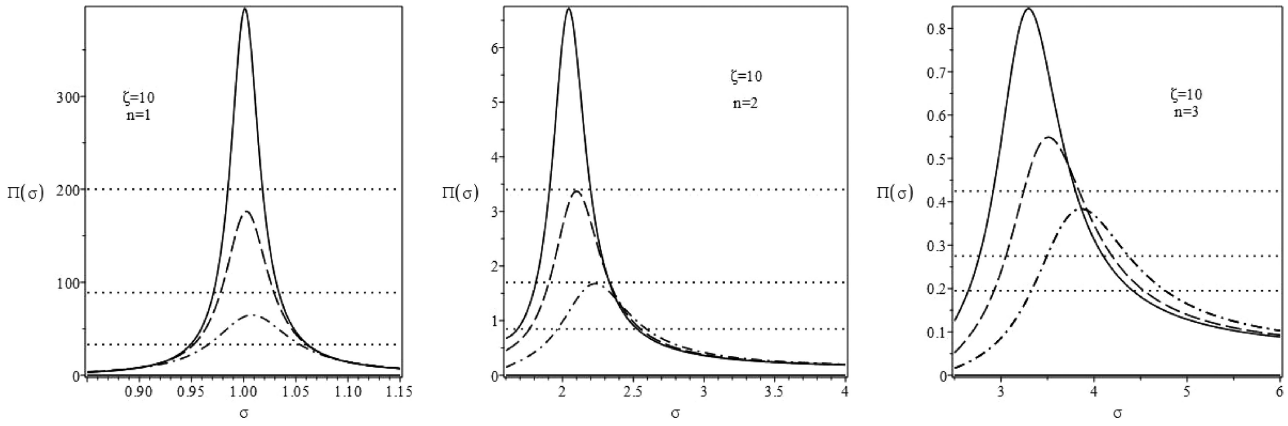

Figure 2. Dependence of Π on σ for $\zeta = 10$. The left-hand, middle, and right-hand panels correspond to $n = 1,\ 2$, and 3, respectively. The solid, dashed, and dash–dotted curves correspond to $\ell = 0.1,\ 0.15$, and 0.25. The dotted horizontal lines show the levels corresponding to the half maximum of $\Pi(\sigma)$.

be used for estimating the coronal atmospheric scale height. When doing so one must take into account the result obtained in this paper that the ratio of the first overtone and fundamental mode deviates from 2 even when there is no density variation along the loop. We recall that we neglected the term proportional to ℓ on the left-hand side of equation (47). However, it is straightforward to see that the account of this term results in the multiplication of eigenfrequencies of both the fundamental harmonic and all overtones by the same multiplier that is slightly different from the unity. Hence, its account cannot change the ratio of frequencies.

We now calculate the average value of $|\eta|^2$ with respect to z. Using

$$\eta = f(t)\frac{L-z}{L} + \sum_{n=1}^{\infty}\eta_n(t)\sin\frac{\pi n z}{L}, \tag{85}$$

we obtain

$$\overline{|\eta|^2} = \frac{1}{L}\int_0^L |\eta|^2\,\mathrm{d}z = \frac{1}{2}\sum_{n=1}^{\infty}|\eta_n(t)|^2 + \frac{1}{3}|f(t)|^2 + \frac{1}{\pi n}\sum_{n=1}^{\infty}(-1)^n[f^*(t)\eta_n(t) + f(t)\eta_n^*(t)], \tag{86}$$

where the asterisk indicates complex conjugate. We introduce the root mean square of η as $\eta_{\mathrm{R}} = \left(\overline{|\eta|^2}\right)^{1/2}$. This quantity can be considered as the measure of the coronal loop displacement. Now, it follows from equation (86) that

$$P_{\eta_{\mathrm{R}}}(\sigma) = \frac{1}{2}\sum_{n=1}^{\infty}P_{\eta_n}(\sigma) + \frac{1}{3}P_f(\sigma) + \frac{2}{\pi n}\sum_{n=1}^{\infty}(-1)^n\Re[P_{f\eta_n}(\sigma)], \tag{87}$$

where $\Re$ indicates the real part of a quantity and $P_{f\eta_n}$ is the cross-correlation function of $f(t)$ and $\eta_n(t)$. We now estimate the terms on the right-hand side of equation (87). We are mainly interested in the value of $P_{\eta_{\mathrm{R}}}(\sigma)$ in the vicinity of resonances, that is in the vicinity of $\sigma = n$. We have already seen that $P_{\eta_n}(\sigma)/P_f(\sigma) = \mathcal{O}(\ell^{-2})$ for $n = 1, 2, 3$. Using the estimate $|P_{f\eta_n}|^2 \le P_{\eta_n}P_f$, we obtain that the ratio of the third term to the first term is of the order of ℓ when σ is in the vicinity of resonances. On the bases of these estimates, we can neglect the second and third terms on the right-hand side of

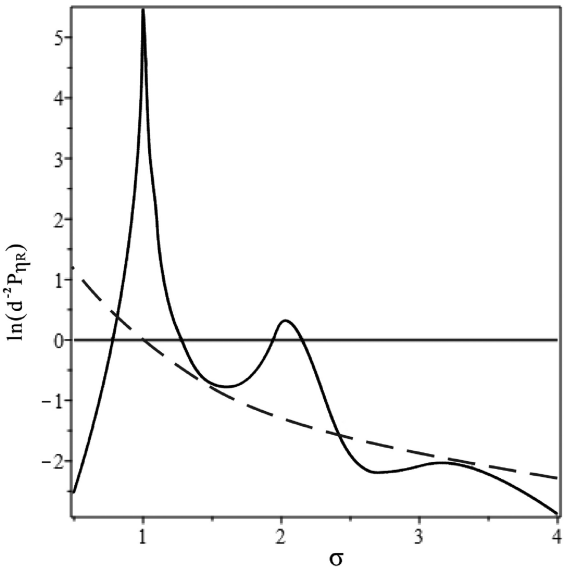

Figure 3. Dependence of $\ln(d^{-2}P_{\eta_{\mathrm{R}}})$ on σ for $\zeta = 3$ and $\ell = 0.15$. The dashed line is the graph of function $\ln(d^{-2}P_f) = -\frac{5}{3}\ln\sigma$.

equation (87) and take

$$P_{\eta_{\mathrm{R}}}(\sigma) \approx \frac{1}{2}\sum_{n=1}^{\infty}P_{\eta_n}(\sigma) = \frac{1}{2}P_f(\sigma)\sum_{n=1}^{\infty}|\Upsilon_n(\sigma)|^2. \tag{88}$$

In the numerical modelling of decayless kink oscillation using the wave equation with damping Afanasyev et al. (2020) assumed that the footpoint displacement is described by a power law with the index $-5/3$. We make the same assumption and take

$$P_f(\sigma) = d^2\sigma^{-5/3}, \quad \sigma \ge \sigma_0, \tag{89}$$

where d is a quantity with the dimension of length, $d \ll R$, and σ_0 is sufficiently small, definitely smaller than $\frac{1}{2}$. Fig. 3 shows the dependence of $\ln(d^{-2}P_{\eta_{\mathrm{R}}})$ on σ for $\zeta = 3$ and $\ell = 0.15$, together with the dependence of the input power on sigma, $\ln(d^{-2}P_f) = -\frac{5}{3}\ln\sigma$. To draw the graph of $P_{\eta_{\mathrm{R}}}(\sigma)$, we used equations (76) and (78). At the boundaries of intervals where there are transitions from expression for $\widetilde{K}(\sigma)$ given by equations (76) to that given by equation (78), or vice versa, this graph contained unphysical spikes. The presence of these peaks is related to the fact that the expressions for $\widetilde{K}(\sigma)$

given by equations (76) and (78) are not valid near the boundaries of the intervals defined by equation (77). To remove these unphysical spikes, we smoothed out the graph near the boundaries of the intervals. We see that the graph has three peaks. The first peak is near $\sigma = 1$. It corresponds to the fundamental mode. The second peak is near $\sigma = 2$. It corresponds to the first overtone. Finally, the third peak is to the right of $\sigma = 3$. It corresponds to the second overtone and it is very weakly pronounced. The first peak is much larger than the second one, and the second peak is in turn much larger than the third one. This is an expected result. What is also worth noting is that the power in the frequency ranges near the fundamental mode frequency and the frequency of the first overtone is strongly enhanced. In contrast, it is not enhanced near the frequency of the second overtone. Rather the power at frequencies slightly different from the frequency of the second overtone is substantially suppressed.

Ruderman & Roberts (2002) and Goossens, Andries & Aschwanden (2002) suggested a method of obtaining the information on the internal structure of coronal loops using the observed damping of kink oscillations. This method is based on the fact that the relative thickness of the transitional layer ℓ is inversely proportional to the damping time. On the basis of results obtained in this article, we can suggest the second method for estimating ℓ based on the observation of decayless kink oscillations. If using the fundamental mode of decayless kink oscillation ($n = 1$), we reproduce its power spectrum then we will be able to estimate $\delta\sigma$. Then it follows from equation (84) that

$$\ell = \frac{8(\delta\sigma)(\zeta + 1)}{\pi(\zeta - 1)}. \tag{90}$$

It would be especially interesting to apply this method when large-amplitude decaying and small-amplitude decayless kink oscillations of the same coronal loop are observed, like in the case reported by Nisticò et al. (2013). In this case, ℓ can be estimated using two different methods and then the results can be compared.

When dealing with observations, we cannot obtained the exact expression for $P_{\eta_n}(\sigma)$ because, in accordance with the definition given by equation (70), for this we need to observe oscillations for infinite time. In reality, the decayless oscillations are only observed during a finite-time period, something between 5 and 10 periods of fundamental kink mode. Hence, we should use the approximate expression for $P_{\eta_n}(\sigma)$ given by equation (70) with $P_{\eta_{Tn}}(\sigma)$ substituted for $P_{\eta_n}(\sigma)$, where T is of the order of a few periods of the fundamental mode. However, this will not affect the estimate for ℓ given by equation (90) because it only depends on $\Upsilon_n(\omega)$.

Since we aim to study the excitation of kink oscillations we do not investigate the plasma motion in the transitional layer. However, it is worth providing a brief discussion of this motion. When the driving is random, there is no single resonant surface. If the spectrum of the driver covers all Alfvén spectrum corresponding to the variation of the Alfvén frequency in the transitional layer, then we can say that any magnetic surface in this layer is a resonant surface. Consequently, there are large gradients in the radial direction in the whole transitional layer. Similar to the case of harmonic driver when the driving begins the oscillation amplitude starts to increase. This increase continues until the average energy dissipation matches the average energy input. However, since now the energy dissipation occurs not in a narrow dissipation layer but in the whole transitional layer, the typical oscillation amplitude is much smaller than that in the case of harmonic driving. Ruderman et al. (1997) studied the direct excitation of torsional Alfvén waves by a harmonic footpoint driving. They found that in the steady state the oscillation amplitude at the resonant surface where the local Alfvén frequency matches the driving frequency is of the order of $\mathrm{Re}^{1/3}$ times the driver amplitude. Ruderman (1999) studied the same problem but with a random driving. He found that in that case the typical oscillation amplitude in the whole transitional layer is of the order of $\mathrm{Re}^{1/6}$ times the driver amplitude. Comparing the driven kink and torsional oscillations, we can make a viable conjecture that the typical oscillation amplitude in the whole transitional layer is of the order of $\mathrm{Re}^{1/6}$ times the driver amplitude also in the case of kink oscillations.

7 SUMMARY AND CONCLUSIONS

In this paper, we studied the excitation of kink oscillations of a magnetic tube by the footpoint driving. We considered the simplest model of a straight magnetic tube homogeneous in the longitudinal direction. There is a thin boundary layer where the density monotonically decreases from its value inside the tube to the value in the surrounding plasma. We used the thin tube and thin boundary (TTTB) approximation. We also used the cold plasma approximation.

The plasma motion is described by the linear ideal MHD equations in the tube and surrounding plasma. However, phase mixing related to the local Alfvén density variation creates large gradients in the radial direction in the boundary layer. This implies that dissipation is important in the boundary layer. Hence, we took viscosity into account when describing motion in this layer. We found an approximate solution to the viscous linear MHD equations in the boundary layer valid for very large Reynolds number. Using this solution, we derived the integro-differential equation governing the magnetic tube kink oscillations.

We used the governing integro-differential equation to study both the harmonic and stochastic driving of the footpoint. In the case of harmonic driving, we reproduced a well-known result that the oscillation amplitude of kink oscillation is of the order of the driver amplitude when the driver is not in resonance with either the fundamental mode or one of the overtones. On the other hand, when there is resonance the oscillation amplitude of kink oscillation is of the order of the driver amplitude divided by the relative thickness of the boundary layer.

In the case of stochastic driving, we assumed that the displacement of the footpoint is described by a stationary random function. This function is characterized by the power spectrum. The tube displacement is the sum of the fundamental mode and all overtones. The amplitudes of the fundamental mode and each overtone are also stationary random functions. We derived the formulae relating the power spectra of the fundamental mode and overtones with the power spectrum of the driver. We assumed that the characteristic scale of variation of the driver power spectrum is of the order of or larger than the fundamental frequency ω_k. This assumption enabled us to take the driver power spectrum to be approximately constant in the vicinity of ω_k and the frequencies of overtones $n\omega_k$, $n = 2, 3, \ldots$ We plot the power spectra of the fundamental mode and the first and second overtones for two values of ratios of the density inside and outside the tube. We also calculated the width of the graph of power spectrum at the height of half of its maximum value and showed that it is proportional to the relative thickness of the transitional layer. On the basis of this result, we suggested a new method of estimation of the transverse structure of coronal loops using the observation of decayless kink oscillations.

First, applications of observations of decayed large-amplitude kink oscillations to coronal seismology used the direct expressions for the

observed quantities. In particular, this approach was used to obtain the information about the transverse structure of coronal magnetic loops using the observed period and damping time of kink oscillations. However, even when the simplest model of a coronal magnetic loop is used, which is a straight magnetic tube where the density only varies in the radial direction, there are three unknown quantities. These are the internal travel Alfvén time, the density contrast, and the ratio of the transitional layer thickness to the loop radius. Since there are only two observed quantities, the oscillation period and damping time, it is only possible to obtain the relation among the three unknown loop parameters. Hence, to estimate the transitional layer thickness the authors made ad hoc assumption about the density contrast.

This fact inspired Arregui & Asensio Ramos (2011) to use Bayesian analysis to improve the reliability of seismological results. Later this method was used by many authors dealing with the coronal seismology (e.g. Arregui, Asensio Ramos & Díaz 2013; Pascoe et al. 2017, 2018; Arregui 2018). I would be convenient to use Bayesian analysis when applying the new method of determination of the internal structure of coronal loops as well. In this way, it would be possible to take into account, for example, the noise and possible temporal variation of the loop parameter. However, the detailed description of application of Bayesian analysis to the seismological method suggested in this paper is only relevant when this method is applied to particular observations.

Finally, we make one comment. For simplicity, we assumed that the loop is driven only at one footpoint. Of course, in the reality the loop is driven at both footpoints as it was considered in the numerical modelling (e.g. Karampelas et al. 2019; Afanasyev et al. 2020). If we consider the loop driving at both footpoints and use the boundary conditions

$$\eta = f_1(t) \quad \text{at} \quad z = 0, \quad \eta = f_2(t) \quad \text{at} \quad z = L,$$

then equation (9) would be changed to

$$\tilde{\xi}_r = \xi_r + \frac{f_1(t)(Z - R) - f_2 Z}{R}.$$

After that again $\tilde{\xi}_r = 0$ at both footpoints. Equation (9) would be changed in a similar way. The first term on the right-hand side of equation (13) would be

$$\frac{Z - R}{R}\frac{\mathrm{d}^2 f_1}{\mathrm{d}t^2} - \frac{Z}{R}\frac{\mathrm{d}^2 f_2}{\mathrm{d}t^2},$$

while the first term on the right-hand side of equation (14) would be given by the same expression multiplied by i. As a result, we would obtain the same expressions for various quantities but with $f_1(t) - f_2(t)$ substituted for $f(t)$. In particular, if we make a viable assumption that the stochastic characteristics of $f_1(t)$ and $f_2(t)$ are the same, then the results obtained in the case of random driving would remain the same.

DATA AVALABILITY

There are no new data associated with this article.

ACKNOWLEDGEMENTS

The authors gratefully acknowledge financial support from the Russian Fund for Fundamental Research (RFFR) grant no. 19-02-00111.

REFERENCES

Abedini A., 2018, Sol. Phys., 293, 22
Afanasyev A. N., Karampelas K., Van Doorsselaere T., 2019, ApJ, 876, 100
Afanasyev A. N., Van Doorsselaere T., Nakariakov V. M., 2020, A&A, 633, L8
Andries J., Arregui I., Goossens M., 2005, ApJ, 624, L57
Andries J., Van Doorsselaere T., Roberts B., Verth G., Verwichte E., Erdélyi R., 2009, Space Sci.Rev., 149, 3
Anfinogentov S. A., Nakariakov V. M., Nisticò G., 2015, A&A, 583, A136
Antolin P., Yokoyama T., Van Doorsselaere T., 2014, ApJ, 787, L22
Antolin P., Moortel I. D., Van Doorsselaere T., Yokoyama T., 2016, ApJ, 830, L22
Arregui I., 2018, Advan. Space Res., 61, 655
Arregui I., Asensio Ramos A., 2011, ApJ, 740, 44
Arregui I., Andries J., Van Doorsselaere T., Goossens M., Poedts S., 2007, A&A, 463, 333
Arregui I., Asensio Ramos A., Ballester J. L., 2013, Living Rev. Sol. Phys., 15, 3
Arregui I., Oliver R., Díaz A. J., 2018, Living Rev. Sol. Phys., 15, 3
Aschwanden M. J., Fletcher L., Schrijver C. J., Alexander D., 1999, ApJ, 520, 880
Bender C. M., Orszag S. A., 1999, Advanced Mathematical Methods for Scientists and Engineers. McGraw-Hill, New York
Champeney D. C., 1973, Fourier Transforms and Their Applications. Academic Press Inc., London
De Groof A., Goossens M., 2000, A&A, 356, 724
De Groof A., Goossens M., 2000, A&A, 335, 329
De Groof A., Goossens M., 2002, A&A, 386, 691
Duckenfield T., Anfinogentov S. A., Pascoe D. J., Nakariakov V. M., 2018, ApJ, 854, L5
Erdélyi R., Taroyan Y., 2008, A&A, 489, L49
Goossens M., Erdélyi R., Ruderman M. S., 1995, Sol. Phys., 157, 75
Goossens M., Andries J., Aschwanden M. J., 2002, A&A, 394, L39
Goossens M., Erdélyi R., Ruderman M. S., 2011, Space. Sci. Rev., 158, 289
Hillier A., Van Doorsselaere T., Karampelas K., 2020, ApJ, 897, L13
Karampelas K., Van Doorsselaere T., Pascoe D. J., Guo M., Antolin P., 2019, Frontiers Astron. Astrophys., 6, 38
Nakariakov V. M., Ofman L., Deluca E. E., Roberts B., Davila J. M., 1999, Science, 285, 862
Nakariakov V. M., Anfinogentov S. A., Nisticò G., Lee D.-H., 2016, A&A, 591, L5
Nisticò G., Nakariakov V. M., Verwichte E., 2013, A&A, 552, A57
Nisticò G., Anfinogentov S., Nakariakov V. M., 2014, A&A, 570, A84
Pascoe D. J., Anfinogentov A. A., Nisticò G., Goddard C. R., Nakariakov V. M., 2017, A&A, 600, A78
Pascoe D. J., Anfinogentov A. A., Goddard C. R., Nakariakov V. M., 2018, ApJ, 860, 31
Ruderman M. S., 1999, ApJ, 521, 851
Ruderman M. S., Roberts B., 2002, ApJ, 577, 475
Ruderman M. S., Berghmans D., Goossens M., Poedts S., 1997, A&A, 615, A156
Ruderman M. S., Verth G., Erdélyi R., 2008, ApJ, 686, 694
Ruderman M. S., Shukhobodskiy A. A., Erdélyi R., 2017, A&A, 602, A50
Shukhobodskiy A. A., Ruderman M. S., 2018, A&A, 615, A156
Su W., Guo Y., Erdélyi R., Ning Z. J., Ding M. D., Cheng X., Tan B. L., 2018, Sci. Rep., 8, 4471
Terradas J., Andries J., Goossens M., Arregui I., Oliver R., Ballester J. L., 2008, ApJ, 687, L115
Terradas J., Magyar N., Van Doorsselaere T., 2018, ApJ, 853, 35
Tian H., McIntosh S. W., Wang T., Ofman L., De Pontieu B., Innes D. E., Peter H., 2012, ApJ, 759, 144
Verth G., Erdélyi R., 2008, A&A, 486, 1015
Verth G., Erdélyi R., Jess D. B., 2008, ApJ, 687, L45
Verwichte E., Nakariakov V. M., Ofman L., Deluca E. E., 2004, Sol. Phys., 223, 77
Wang T. J., Ofman L., Davila J., Yang S., 2012, ApJ, 751, L27

APPENDIX A: EVALUATION OF THE RIGHT-HAND SIDE OF EQUATION (47)

In this section, we transform the right-hand side of equation (47). Using equations (41) and (45), we rewrite the expression given by equation (35) as

$$\delta\eta_n = -n^2 W_1 - \frac{2}{\pi} W_2, \tag{A1}$$

where

$$W_1 = \frac{n^2(\varpi_k^2 - \omega_{Ai}^2)}{R} \int_{R(1-\ell/2)}^{R(1+\ell/2)} \frac{\rho_i}{\rho}\, \mathrm{d}r \times \int_{-\infty}^{t} \widetilde{G}_n(t-\theta)\eta_n(\theta)\, \mathrm{d}\theta, \tag{A2}$$

$$W_2 = \frac{1}{\pi n R} \int_{R(1-\ell/2)}^{R(1+\ell/2)} \mathrm{d}r \int_{-\infty}^{t} \widetilde{G}_n(t-\theta) \frac{\mathrm{d}^2 f}{\mathrm{d}\theta^2}\, \mathrm{d}\theta, \tag{A3}$$

and $\widetilde{G}_n(t-\theta)$ is defined by

$$\widetilde{G}_n(t) = \exp\left(-n^2(t/t_d)^3\right) \frac{\sin(n\omega_{\mathrm{A}} t)}{n\omega_{\mathrm{A}}}, \quad t_d^{-3} = \frac{\nu}{6}\left(\frac{\mathrm{d}\omega_{\mathrm{A}}}{\mathrm{d}r}\right)^2. \tag{A4}$$

Differentiating this expression, we obtain

$$\widetilde{G}_n'(t) = \exp\left(-n^2(t/t_{\mathrm{d}})^3\right)\cos(n\omega_{\mathrm{A}} t) - \frac{3n^2t^2}{t_d^3}\widetilde{G}_n(t), \tag{A5}$$

$$\widetilde{G}_n''(t) = -n^2\omega_{\mathrm{A}}^2\widetilde{G}_n(t) + \frac{3n^2 t}{t_d^3}\left[\widetilde{G}_n(t)\left(\frac{3n^2t^3}{t_d^3} - 2\right) - 2t\exp\left(-n^2(t/t_d)^3\right)\cos(n\omega_{\mathrm{A}} t)\right], \tag{A6}$$

where the prime indicates the derivative. We will also use the prime to indicate the derivative of $\widetilde{G}_n(t-\theta)$ with respect to the argument. Below we use the relation

$$\frac{\partial \widetilde{G}_n(t-\theta)}{\partial\theta} = -\frac{\partial \widetilde{G}_n(t-\theta)}{\partial t} = -\widetilde{G}_n'(t-\theta). \tag{A7}$$

Using the integration by parts and equations (A4) and (A7), we obtain

$$\int_{-\infty}^{t} \widetilde{G}_n(t-\theta)\frac{\mathrm{d}^2 f}{\mathrm{d}\theta^2}\mathrm{d}\theta = \int_{-\infty}^{t} \widetilde{G}_n'(t-\theta)\frac{\mathrm{d}f}{\mathrm{d}\theta}\mathrm{d}\theta. \tag{A8}$$

Again using the integration by parts and equations (A5) and (A7) yields

$$\int_{-\infty}^{t} \widetilde{G}_n'(t-\theta)\frac{\mathrm{d}f}{\mathrm{d}\theta}\,\mathrm{d}\theta = f(t) + \int_{-\infty}^{t} \widetilde{G}_n''(t-\theta) f(\theta)\,\mathrm{d}\theta. \tag{A9}$$

With the aid of equations (A6), (A8), and (A9), we obtain

$$\int_{-\infty}^{t} \widetilde{G}_n(t-\theta)\frac{\mathrm{d}^2 f}{\mathrm{d}\theta^2}\mathrm{d}\theta = -n^2\omega_A^2 \int_{-\infty}^{t} \widetilde{G}_n(t-\theta) f(\theta)\,\mathrm{d}\theta + f(t) + \frac{3n^2}{t_d^3}\int_{-\infty}^{t} f(\theta)(t-\theta)\left\{\widetilde{G}_n(t-\theta) \times \left(\frac{3n^2(t-\theta)^3}{t_d^3} - 2\right) - 2(t-\theta) \times \exp\left(-n^2(t-\theta)^3/t_{\mathrm{d}}^3\right)\cos[n\omega_A(t-\theta)]\right\}\mathrm{d}\theta. \tag{A10}$$

It is straightforward to show that the ratio of the third term to the second one on the right-hand side of this equation is of the order of Re^{-1}. Hence, we can neglect the third term and use the approximate relation

$$W_2 \approx \frac{\ell f(t)}{n} - \frac{n}{R}\int_{R(1-\ell/2)}^{R(1+\ell/2)} \omega_{\mathrm{A}}^2\,\mathrm{d}r \int_{-\infty}^{t} \widetilde{G}_n(t-\theta) f(\theta)\,\mathrm{d}\theta. \tag{A11}$$

Differentiating this expression, we obtain

$$\frac{\mathrm{d}^2 W_2}{\mathrm{d}t^2} = \frac{\ell}{n}\frac{\mathrm{d}^2 f}{\mathrm{d}t^2} - \frac{n}{R}\int_{R(1-\ell/2)}^{R(1+\ell/2)} \omega_A^2\,\mathrm{d}r\left[f(t) + \int_{-\infty}^{t} f(\theta)\widetilde{G}_n''(t-\theta)\right]\mathrm{d}\theta. \tag{A12}$$

Using equation (A7) twice yields

$$\int_{-\infty}^{t} f(\theta)\widetilde{G}_n''(t-\theta)\big]\,\mathrm{d}\theta = \int_{-\infty}^{t} f(\theta)\frac{\partial^2 \widetilde{G}_n(t-\theta)}{\partial\theta^2}\,\mathrm{d}\theta. \tag{A13}$$

Using the integration by parts and equation (A5), we obtain

$$\int_{-\infty}^{t} f(\theta)\frac{\partial^2 \widetilde{G}_n(t-\theta)}{\partial\theta^2}\,\mathrm{d}\theta = f(t) - \int_{-\infty}^{t} \frac{\partial \widetilde{G}_n(t-\theta)}{\partial\theta}\frac{\mathrm{d}f}{\mathrm{d}\theta}\,\mathrm{d}\theta. \tag{A14}$$

Using again the integration by parts and equation (A4) yields

$$\int_{-\infty}^{t} \frac{\partial \widetilde{G}_n(t-\theta)}{\partial\theta}\frac{\mathrm{d}f}{\mathrm{d}\theta}\,\mathrm{d}\theta = -\int_{-\infty}^{t} \widetilde{G}_n(t-\theta)\frac{\mathrm{d}^2 f}{\mathrm{d}\theta^2}\,\mathrm{d}\theta. \tag{A15}$$

With the aid of equations (A13)–(A15), we obtain

$$\int_{-\infty}^{t} f(\theta)\frac{\mathrm{d}^2 \widetilde{G}_n(t-\theta)}{\mathrm{d}t^2}\mathrm{d}\theta = \int_{-\infty}^{t} \widetilde{G}_n(t-\theta)\frac{\mathrm{d}^2 f}{\mathrm{d}\theta^2}\mathrm{d}\theta - f(t). \tag{A16}$$

Substituting equation (A16) in equation (A12) yields

$$\frac{\mathrm{d}^2 W_2}{\mathrm{d}t^2} = \frac{\ell}{n}\frac{\mathrm{d}^2 f}{\mathrm{d}t^2} - \frac{n}{R}\int_{R(1-\ell/2)}^{R(1+\ell/2)} \omega_A^2\,\mathrm{d}r \times \int_{-\infty}^{t} \widetilde{G}_n(t-\theta)\frac{\mathrm{d}^2 f}{\mathrm{d}\theta^2}\,\mathrm{d}\theta. \tag{A17}$$

Next, using equation (A7) twice, and equations (A4) and (A5), we obtain

$$\frac{\mathrm{d}^2}{\mathrm{d}t^2}\int_{-\infty}^{t} \widetilde{G}_n(t-\theta)\eta_n(\theta)\,\mathrm{d}\theta = \eta_n(t) + \int_{-\infty}^{t} \frac{\partial^2 \widetilde{G}_n(t-\theta)}{\partial\theta^2}\eta_n(\theta)\,\mathrm{d}\theta. \tag{A18}$$

Using the integration by parts twice, and equations (A4) and (A5) yields

$$\int_{-\infty}^{t} \frac{\partial^2 \widetilde{G}_n(t-\theta)}{\partial\theta^2}\eta_n(\theta)\,\mathrm{d}\theta = \int_{-\infty}^{t} \widetilde{G}_n(t-\theta)\frac{\mathrm{d}^2\eta_n}{\mathrm{d}\theta^2}\,\mathrm{d}\theta - \eta_n(t). \tag{A19}$$

Finally, using equations (44), (A18), and (A19), we arrive at

$$\frac{\mathrm{d}^2}{\mathrm{d}t^2}\int_{-\infty}^{t} \widetilde{G}_n(t-\theta)\eta_n(\theta)\,\mathrm{d}\theta = \int_{-\infty}^{t} \widetilde{G}_n(t-\theta)\frac{\mathrm{d}^2\eta_n}{\mathrm{d}\theta^2}\,\mathrm{d}\theta \approx -n^2\varpi_k^2\int_{-\infty}^{t} \widetilde{G}_n(t-\theta)\eta_n(\theta)\,\mathrm{d}\theta. \tag{A20}$$

It follows from this result that

$$\frac{\mathrm{d}^2 W_1}{\mathrm{d}t^2} = -n^2\varpi_k^2 W_1. \tag{A21}$$

Now using equations (A1)–(A3), (A17), and (A21) yields

$$\frac{\mathrm{d}^2\delta\eta_n}{\mathrm{d}t^2}+\omega_{Ae}^2n^2\delta\eta_n=\frac{n^6}{R}\rho_i(\varpi_k^2-\omega_{Ae}^2)(\varpi_k^2-\omega_{Ai}^2)\times\int_{R(1-\ell/2)}^{R(1+\ell/2)}\frac{\mathrm{d}r}{\rho}\int_{-\infty}^{t}\widetilde{G}_n(t-\theta)\eta_n(\theta)\,\mathrm{d}\theta-\frac{2\ell}{\pi n}\frac{\mathrm{d}^2f}{\mathrm{d}t^2}-\frac{2n}{\pi R}\int_{R(1-\ell/2)}^{R(1+\ell/2)}(\omega_{Ae}^2-\omega_{\mathrm{A}}^2)\,\mathrm{d}r\int_{-\infty}^{t}\widetilde{G}_n(t-\theta)\frac{\mathrm{d}^2f}{\mathrm{d}\theta^2}\mathrm{d}\theta. \tag{A22}$$

APPENDIX B: CALCULATION OF INTEGRAL IN EQUATION (57)

In this section, we calculate the integral in equation (57) in the case when the driver is in resonance with one of harmonics, $\omega_d = n\varpi_k$. Using equation (52), we obtain the estimate

$$t_d\omega_d(3n^2)^{-1/3}\sim(\ell^2\mathrm{Re})^{1/3}. \tag{B1}$$

We assume that $\ell^2\mathrm{Re}\gg1$. Using the integration by parts we easily obtain that

$$F(x)=\frac{i}{x}+\mathcal{O}\big(1/x^2\big) \tag{B2}$$

for $|x|\gg1$. It follows from equation (59) that $t_d(3n^2)^{-1/3}(\omega_d+n\omega_{\mathrm{A}})\gg1$. This implies that we can use the approximate expression given by equation (B2) to calculate the second term in the square brackets in the expression for ψ_n given by equation (54). Since $\varpi_k\in(\omega_{Ai},\omega_{Ae})$, it follows that there is such a point $r=r_{\mathrm{A}}$ that $n\omega_{\mathrm{A}}(r_A)=\omega_d=n\varpi_k$. This is the point of Alfvén resonance. Hence, $t_d(3n^2)^{-1/3}|\omega_d-n\omega_{\mathrm{A}}|\gg1$ only for r not very close to r_A. The exact condition is $|r-r_{\mathrm{A}}|\gg\ell R(\ell^2\mathrm{Re})^{-1/3}$. When this condition is satisfied we have

$$\psi_n\approx\frac{i\omega_{\mathrm{A}}}{n(\varpi_k^2-\omega_{\mathrm{A}}^2)}. \tag{B3}$$

This quantity is singular at $r=r_A$. We introduce $(\ell^2\mathrm{Re})^{-1/3}\ll\chi\ll1$. equation (B3) is valid when $|r-r_{\mathrm{A}}|\geq\chi lR$. When $|r-r_A|\leq\chi\ell R$ all quantities in the integrand in the integral in equation (57) can be approximated by the first term of its expansion in the Taylor series. In particular,

$$n\omega_{\mathrm{A}}-\omega_d\approx-n\Delta(r-r_A),\quad\Delta=-\left.\frac{\mathrm{d}\omega_{\mathrm{A}}}{\mathrm{d}r}\right|_{r=r_{\mathrm{A}}}. \tag{B4}$$

Then for $|r-r_A\ell|\leq\chi\ell R$, we have

$$\psi_n(\omega_d)\approx-\frac{i}{4n\varpi_k}-\frac{\bar{t}_d}{2(3n^2)^{1/3}}F\big(\bar{t}_d(n/3)^{1/3}\Delta(r_{\mathrm{A}}-r)\big), \tag{B5}$$

where $\bar{t}_d$ is the value of t_d calculated at $r=r_{\mathrm{A}}$. Now, we obtain an approximate expression

$$\int_{R(1-\ell/2)}^{R(1+\ell/2)}\omega_{\mathrm{A}}\psi_n(\omega_d)\,\mathrm{d}r\approx\frac{i}{n}\left(\int_{R(1-\ell/2)}^{r_{\mathrm{A}}-\chi\ell R}+\int_{r_{\mathrm{A}}+\chi\ell R}^{R(1+\ell/2)}\right)\frac{\omega_{\mathrm{A}}^2\,\mathrm{d}r}{\varpi_k^2-\omega_{\mathrm{A}}^2}-\frac{i\chi\ell R}{2n}-\frac{\bar{t}_d\varpi_k}{2(3n^2)^{1/3}}\int_{r_{\mathrm{A}}-\chi\ell R}^{r_{\mathrm{A}}+\chi\ell R}F\big(\bar{t}_d(n/3)^{1/3}\Delta(r_{\mathrm{A}}-r)\big)\,\mathrm{d}r. \tag{B6}$$

Using the expression for $F(x)$ given by equation (56) and changing the order of integration in the last integral yields

$$\int_{r_A-\chi\ell R}^{r_{\mathrm{A}}+\chi\ell R}F\big(\bar{t}_{\mathrm{d}}(n/3)^{1/3}\Delta(r_{\mathrm{A}}-r)\big)\,\mathrm{d}r=\frac{-1}{\bar{t}_d|\Delta|(n/3)^{1/3}}\times\int_0^{\infty}\mathrm{e}^{-\theta^3/3}\sin\big(\chi\bar{t}_{\mathrm{d}}\ell R|\Delta|(n/3)^{1/3}\theta\big)\frac{\mathrm{d}\theta}{\theta}. \tag{B7}$$

It follows from equation (B1) and the inequality $\chi\gg(\ell^2\mathrm{Re})^{-1/3}$ that

$$\varepsilon^{-1}=\chi\bar{t}_d\ell R|\Delta|(n/3)^{1/3}\gg1. \tag{B8}$$

Then we obtain

$$\int_0^{\infty}\mathrm{e}^{-\theta^3/3}\sin\big(\chi\bar{t}_{\mathrm{d}}\ell R|\Delta|(n/3)^{1/3}\theta\big)\frac{\mathrm{d}\theta}{\theta}=\int_0^{\infty}\frac{\sin\theta}{\theta}\mathrm{e}^{-\varepsilon^3\theta^3/3}\mathrm{d}\theta=\int_0^{\infty}\frac{\sin\theta}{\theta}\mathrm{d}\theta+\mathcal{O}(\varepsilon^3)\approx\frac{\pi}{2}. \tag{B9}$$

Using equations (B7) and (B9) and taking formally $\chi\to0$, we obtain from equation (B6)

$$\int_{R(1-\ell/2)}^{R(1+\ell/2)}\omega_A\psi_n(\omega_{\mathrm{d}})\,\mathrm{d}r\approx\frac{i}{n}\mathcal{P}\int_{R(1-\ell/2)}^{R(1+\ell/2)}\frac{\omega_{\mathrm{A}}^2\,\mathrm{d}r}{\varpi_k^2-\omega_{\mathrm{A}}^2}+\frac{\pi\varpi_k}{4n|\Delta|}, \tag{B10}$$

where $\mathcal{P}$ indicates that the integral is calculated in the sense of the Cauchy principal part. Substituting this expression in equation (57) with $\omega_d=n\varpi_k$, we arrive at equation (59).

APPENDIX C: CALCULATION OF THE FOURIER TRANSFORM OF $\hat{L}[\eta_n]$

We rewrite equation (51) as

$$\hat{L}[\eta_n]=-\frac{n^5\varpi_k^2(\rho_i-\rho_e)^2}{2R(\rho_i+\rho_e)^2}\int_{R(1-\ell/2)}^{R(1+\ell/2)}\omega_A\Xi(t)\,\mathrm{d}r, \tag{C1}$$

where

$$\Xi(t)=\int_{-\infty}^{t}\exp\big(-n^2(t-\theta)^3/t_d^3\big)\sin[n\omega_A(t-\theta)]\eta_n(\theta)\,\mathrm{d}\theta. \tag{C2}$$

We calculate the Fourier transform of $\Xi(t)$:

$$\hat{\Xi}(\omega)=\int_{-\infty}^{\infty}e^{-i\omega t}\mathrm{d}t\int_{-\infty}^{t}\exp\big(-n^2(t-\theta)^3/t_{\mathrm{d}}^3\big)\times\sin[n\omega_A(t-\theta)]\eta_n(\theta)\,\mathrm{d}\theta. \tag{C3}$$

Changing the order of integration in this double integral yields

$$\hat{\Xi}(\omega)=\int_{-\infty}^{\infty}\eta_n(\theta)\,\mathrm{d}\theta\int_{\theta}^{\infty}\mathrm{e}^{-i\omega t}\exp\big(-n^2(t-\theta)^3/t_d^3\big)\times\sin[n\omega_{\mathrm{A}}(t-\theta)]\,\mathrm{d}t. \tag{C4}$$

Using the variable substitution $t=\tilde{t}+\theta$ and dropping the tilde yields

$$\hat{\Xi}(\omega)=\int_{-\infty}^{\infty}\eta_n(\theta)\mathrm{e}^{-i\omega\theta}\,\mathrm{d}\theta\times\int_0^{\infty}\exp\big(-i\omega t-n^2t^3/t_d^3\big)\sin(n\omega_{\mathrm{A}}t)\,\mathrm{d}t. \tag{C5}$$

The substitution $t=t_d(3n^2)^{-1/3}\theta$ reduces this expression to

$$\hat{\Xi}(\omega)=i\psi_n(\omega)\hat{\eta}_n(\omega). \tag{C6}$$

It follows from equations (C1) and (C6) that

$$\mathcal{F}\big(\hat{L}[\eta_n]\big)=i\hat{\eta}_n(\omega)K(\omega), \tag{C7}$$

where

$$K(\omega)=-\frac{n^5\varpi_k^2(\rho_i-\rho_e)^2}{2R(\rho_i+\rho_e)^2}\int_{R(1-\ell/2)}^{R(1+\ell/2)}\omega_A\psi_n(\omega)\,\mathrm{d}r. \tag{C8}$$

Now, we simplify the expression for $K(\omega)$ valid for $\ell^2\mathrm{Re}\gg1$. We can use the same derivation as in Appendix B with the only difference

that there is the point $r_n(\omega)$ defined by $n\omega_{\rm A}(r_n) = \omega$ only when $\omega \in [n\omega_{Ai}, n\omega_{Ae}]$. When this condition is satisfied, we obtain the equation similar to equation (B10) but with ω/n substituted for ϖ_k and Δ_n substituted for Δ, where $\Delta_n = -n{\rm d}\omega_{\rm A}/{\rm d}r$ calculated at r_n. When $\omega \in [n\omega_{Ai}, n\omega_{Ae}]$, the term similar to the second term on the right-hand side of equation (B10) is absent. Hence,

$$\int_{R(1-\ell/2)}^{R(1+\ell/2)} \omega_{\rm A}\psi_n(\omega_d)\,{\rm d}r \approx -\frac{\pi\omega}{4n^2\Delta_n} + in\mathcal{P}\int_{R(1-\ell/2)}^{R(1+\ell/2)} \frac{\omega_{\rm A}^2\,{\rm d}r}{\omega^2 - n^2\omega_{\rm A}^2}, \quad \omega \in [n\omega_{Ai}, n\omega_{Ae}], \tag{C9}$$

$$\int_{R(1-\ell/2)}^{R(1+\ell/2)} \omega_{\rm A}\psi_n(\omega)\,{\rm d}r \approx \approx in\mathcal{P}\int_{R(1-\ell/2)}^{R(1+\ell/2)} \frac{\omega_{\rm A}^2\,{\rm d}r}{\omega^2 - n^2\omega_{\rm A}^2}, \quad \omega \notin [n\omega_{Ai}, n\omega_{Ae}]. \tag{C10}$$

Substituting equations (C9) and (C10) in equation (64), we obtain equations (65) and (66).

This paper has been typeset from a TEX/LATEX file prepared by the author.